ASM Sc. J., 17, 2022

https://doi.org/10.32802/asmscj.2022.968

Automated Knee Bone Segmentation and Visualisation Using Mask RCNN and Marching Cube: Data From The Osteoarthritis Initiative

Rahul Patekar[1], Prashant Shukla Kumar[2], Hong-Seng Gan[3*] and Muhammad Hanif Ramlee[4]

[1]*Electronics and Telecommunication Engineering Department, Shri Guru Gobind Singhji Institute of Engineering and Technology, Nanded, Maharashtra, India*

[2]*Medical Engineering Technology Section, British Malaysian Institute, Universiti Kuala Lumpur, 53100 Gombak, Malaysia*

[3]*Department of Data Science, Universiti Malaysia Kelantan, 16100 UMK City Campus, Pengkalan Chepa, Kelantan, Malaysia*

[4]*Bioinspired Devices and Tissue Engineering (BIOINSPIRA) Group, School of Biomedical Engineering and Health Sciences, Faculty of Engineering, University Teknologi Malaysia, 81310 UTM Johor Bahru, Malaysia*

In this work, an automated knee bone segmentation model is proposed. A mask region-based convolutional neural network (RCNN) algorithm is developed to segment the bone and reconstructed into 3D object by using Marching-Cube algorithm. The proposed method is divided into two stages. First, the Mask RCNN is introduced to segment subchondral knee bone from the input MRI sequence. In the second stage, the segmented output from Mask R-CNN is fed as input to the Marching cube algorithm for the 3D reconstruction of knee subchondral bone. The proposed method achieved high dice similarity scores for femur bone 95.35%, tibia bone 95.3%, and patella bone 94.40% using a Mask R-CNN with Resnet-50 as backbone architecture. Improved dice similarity scores for femur bone 97.11%, tibia bone 97.33%, and patella bone 97.05% are obtained by Mask RCNN with Resnet-101 as backbone architecture. It is noted that the Mask RCNN framework has demonstrated efficient and accurate knee subchondral bone detection as well as segmentation for input MRI sequences.

Keywords: Mask Region-based Convolutional Neural Network; Osteoarthritis, Magnetic resonance imaging; Knee Bone Segmentation

I. INTRODUCTION

Osteoarthritis (OA) is a chronic disease mostly diagnosed in the knee joints of elderly, female, and overweight people. OA responsible for 2.4% of all years lived with disability and was ranked as the 10th leading contributor to global years lived with disability. The monitoring of knee-osteoarthritis progression is possible by measuring pre-structural and structural changes associated with ligaments, articular cartilage, meniscus, subchondral bones, and synovial fluid. Although most of the OA evaluations are based on simple radiographic assessment techniques (X-ray), researchers have demonstrated that knee OA can effectively measure by utilising Magnetic Resonance (MR) Imaging (Hong-Seng *et al.,* 2017). The relationship between the progression of knee OA and changes in the shape of knee subchondral bone is reported by the Foundation of National Institute of Health osteoarthritis biomarkers consortium. Therefore, knee subchondral bone segmentation methods have received increasing attention. In recent years, methods based on convolutional neural networks (CNNs) have led to dramatic improvements in knee subchondral bone detection and segmentation methods (Hong-Seng *et al.,* 2020).

Liu *et al.* (2018) described Deep CNN and 3D Deformable pipeline for pixel-wise multi-class cartilage and bone

*Corresponding author's e-mail: hongseng.g@umk.edu.my

classification. In Liu *et al.* (2018) work, the SegNet framework (Deep CNN) was selected as the automated bone and cartilage segmentation. The 3D deformable technique was used to create a smooth surface for musculoskeletal structures. Deniz *et al.* (2018) presented an automatic proximal femur segmentation algorithm based on 2D and 3D deep CNNs. Lee *et al.* (2018) presented the BCD-NET method cartilage segmentation using bone-BCC difference (BCD) extraction and bone-cartilage-complex (BCC) approach. The performance of the BCD-Network was improved by using multi-view 2.5D segmentation on three orthogonal planes namely sagittal (S), coronal (C), and axial (A) planes.

Zhou *et al.* (2018) presented a segmentation algorithm consisted of CNN, 3D fully connected conditional random field (CRF), and 3D simplex deformable approach. The combined architecture was used to improve the performance of knee joint tissue segmentation. Ambellan *et al.* (2019) introduced a robust and accurate segmentation of bone and cartilage consisting of 3D Statistical Shape Models (SSMs) adjustment, 2D U-Net, 3D U-Net, and SSM post-processing pipeline. This paper presented a fully automated segmentation method for knee bone and cartilage by combining the advantages of SSM-based regularisation with CNN-based classification of voxel intensities. However, existing U-Net (Deniz *et al.,* 2018), SegNet (Liu *et al.,* 2018), RetinaNet (Lin *et al.,* 2017), BCD-NET (Lee *et al.,* 2018) and other deep stacking networks (DSN) are facing spatial information loss due to a semantic gap between the corresponding levels of encoder-decoder for knee bone segmentation. Besides, these methods suffer from poor segmentation performance for smaller ROIs.

In this research work, a mask region-based convolutional neural network (R-CNN) He *et al.* (2017) framework is developed for knee subchondral bone detection, localisation, and segmentation from MR images. The Mask R-CNN framework produces a more accurate segmentation mask for each bone instance due to the backbone network, Feature Pyramid Network (FPN), Region Proposal Network (RPN), Region of Interest (ROI) Classifier & Bounding Box Regression and Segmentation Masks as building processing block. Each processing block in Mask R-CNN is responsible to detect, localise, segment knee subchondral bone from different image appearances, imaging artifacts of multiple MRI sequences. Mask R-CNN network preserves spatial information for knee bone instance segmentation because there is no semantic gap between encoder-decoder stages. The 3D subchondral bone generated from the output of the marching cube model was used to predict the risk of developing knee osteoarthritis and to detect osteoarthritis progression up to the knee replacement stage (Gait *et. al.,* 2016; Mackay *et al.,* 2017).

The structure of paper is organised as follow: Section II explains the materials and methods, Section III describes the experimental results of knee subchondral bone segmentation and 3D visualisation and Section IV concludes the work.

II. METHODOLOGY

A. Image Dataset

MR image of knee from the Osteoarthritis Initiative (OAI) (Peterfy *et al.,* 2008), dataset was used to train and test the knee bone segmentation model.

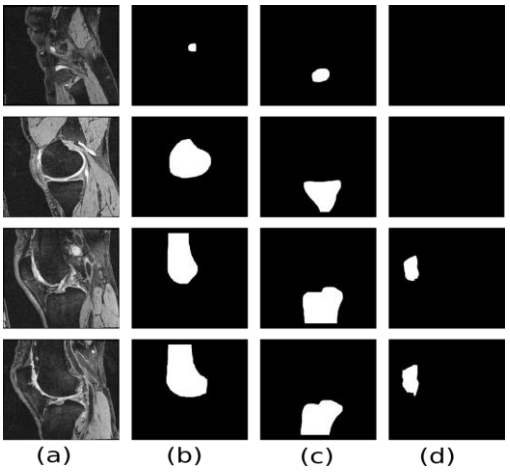

Figure 1. Original image with the ground-truths. (a) MR image sequence, (b) Femur bone mask, (c) Tibia bone mask, and (d) Patella bone mask

Figure 1 shows the MR image with ground-truth labels for each class. The MR image sequences were captured by using double echo steady-state (DESS) in the sagittal plane with the following specification details: matrix size of 384x384, in-plane resolution of 0.36x0.365 mm, slice thickness of 0.7 mm, a repetition time/echo time of 16.3/4.7 ms, flip angle of 25, and bandwidth (BW) of 185 Hz/pixel, and field-of-view of 140x140 mm. To perform Knee bone segmentation and 3D

visualisation, the MR images and their respective ground truth mask play an important role.

B. Architecture of the Proposed Knee Bone Segmentation

The R-CNN (Girshick *et al.,* 2014), a fast R-CNN (Girshick *et al.,* 2015) and faster R-CNN (Ren *et al.,* 2015) are the deep neural network to show that CNNs can achieve better object detection performance on the PASCAL VOC Challenge. But the R-CNN model is computationally difficult to train due to its architecture complexity and fast R-CNN model required selective search as bottleneck process. It was observed that Faster R-CNN has poor performance for pixel-level object classification.

In this work Mask R-CNN algorithm is introduced for knee subchondral bone segmentation. The process flow of the subchondral bone segmentation model is depicted in Figure 2. The proposed algorithm is consisting of two stages namely subchondral bone segmentation and 3D visualisation. In the first stage, MR images with ground truth labels are provided as input to the Mask R-CNN. Here, Mask R-CNN is used to generate the three types of output such as Class label, bounding box (BBox), a segmented mask for knee bone. In the second stage, the segmented knee subchondral bone mask from 160 samples are collectively used for 3D visualisation.

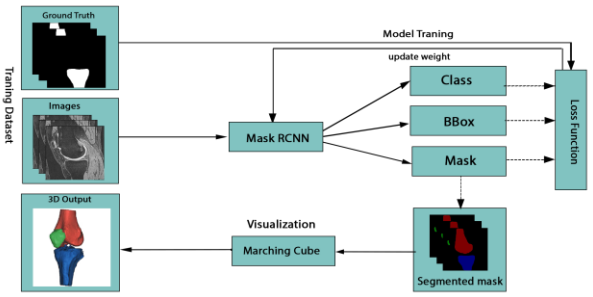

Figure 2. Process flow of the proposed Mask R-CNN subchondral bone segmentation model

C. Subchondral Bone Segmentation

The Mask R-CNN framework consists of two steps; the first step generates the proposal which likely to contain a knee subchondral bone from the input MR image. The second step predicted the class of generated proposals, created masks, and bounding box for input MR image. Figure 3 illustrates the different processing block of Mask R-CNN algorithm.

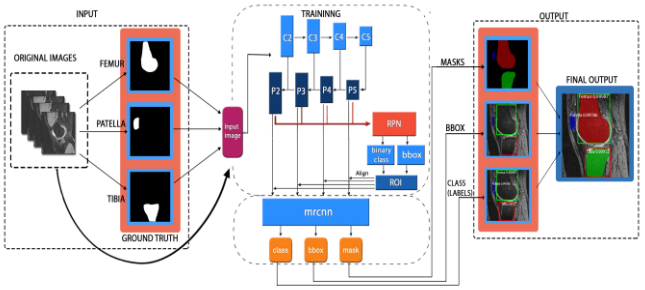

Figure 3. Subchondral Bone Segmentation using Mask R-CNN algorithm

Mask R-CNN consists of ResNet50 or ResNet101 and Feature Pyramid Network (FPN) as backbone modules. The Resnet-50 or Resnet-101 network was introduced to tackle vanishing gradient with the help of a residual block and represented as:

$$Y = F(x, W_i) + W_{sx} \qquad (1)$$

The identity mapping is multiplied by a linear projection W to expand the channels of shortcut to match the residual. This allows for the input x and F(x) to be combined as input to the next layer. However, the Feature pyramid network takes a single-scale image of arbitrary size as input, and outputs proportionally sized feature maps at multiple levels, in a fully convolutional fashion with the help of the following equation. Here 384 is the size of the input MR image, and k_0 is the target level on which a ROI with w × h = 384×384 should be mapped. The algorithm uses the size of the 256 top-down layers to create features pyramid.

$$k = k_0 + \log_2(wh)\,\mathrm{x}\,384 \qquad (2)$$

The Region Proposal Network (RPN) scans over the backbone feature map in a sliding window fashion and predicts the ROI that likely contains knee subchondral bone (Anchors). The predicted region proposals are then reshaped using a ROI align layer which is then used to classify the image within the proposed region and predict the offset values for the bounding boxes. The ROI Classifier & Bounding Box Regressor module runs on ROI that contains subchondral bone to predict two outputs (i.e. output class and

BBox regressor) for each ROI in the Knee MR image provided by RPN. Mask R-CNN generates a mask for each class separately and the loss function is used per pixel sigmoid and binary loss.

$$L = L_{cls} + L_{box} + L_{mask} \quad (3)$$

The multi-task loss function L of Mask R-CNN is the addition of the loss of classification L_{cls}, localisation L_{box} and segmentation mask L_{mask} during the training on each sampled ROI that makes Mask R-CNN more accurate. It is noted that the Mask R-CNN is used for providing significantly improved results than State-of-the-art methods for subchondral bone segmentation.

D. 3D Visualisation using a Marching Cube Algorithm

The segmented output is then used to for 3D visualisation in computer-aid diagnosis, architecture, medicals, and related areas by Volume rendering techniques namely marching cube algorithm [21]. The marching cube algorithm is divided into two stages. First, the algorithm locates the surface corresponding to a user-specified value and creates triangles. Second, to ensure a quality image of the surface, then calculate the normal to the surface at each vertex of each triangle. The algorithm scans two slices of images and creates a logical cube with four neighbouring pixels from both slices. The eight density value at the cube vertex is used to calculate the cube index. The cube index is considered as a pointer in the edge table to determine all edge intersections. To calculate the intersection points it requires to do linear interpolation:

$$P = P1 + (iso\_level - v1)*(P2 - P1)/(v2 - v1) \quad (4)$$

The linear interpolation is used to interpolate surface intersection along the edge. If P1 and P2 are the vertices of a cut edge and v1 and v2 are the scalar values at each vertex, the intersection point P is given by equation 4. After calculating Interpolate surface intersection along each edge, Algorithm Calculate normal for each cube vertex using central differences:

$$G_x(i, j, k) = \frac{D(i+1, j, k) - D(i-1, j, k)}{\Delta x} \quad (5)$$

$$G_y(i, j, k) = \frac{D(i, j+1, k) - D(i, j-1, k)}{\Delta y} \quad (6)$$

$$G_z(i, j, k) = \frac{D(i, j, k+1) - D(i, j, k-1)}{\Delta z} \quad (7)$$

Where D (i, j, k) is the density at pixel (i, j) in slice k and Δx, Δy, Δz are the lengths of the cube edges. The final step in a marching cube algorithm is to interpolate the normal at the vertices of the triangles and mathematically it is representing as:

$$n_1 = ug_2 + (1 - u)g_1 \quad (8)$$

A three-dimensional representation of the subchondral bone can be visualised by drawing these triangles. Figure 4 shows the basic pipeline of 3D modelling using the Marching cube.

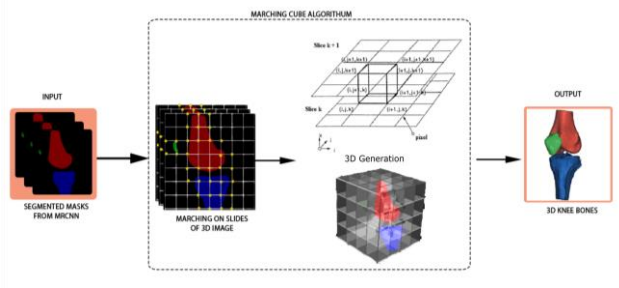

Figure 4. 3D reconstruction using the Marching cube algorithm

III. RESULTS AND DISCUSSION

A. Evaluation Metrics

To obtain accurate 3D bone surface reconstruction, it is required to achieve accurate instance bone segmentation. Dice similarity coefficient (DSC), sensitivity and specificity are the benchmark evaluation matrices in knee segmentation model evaluation (Hong-Seng *et al.,* 2019). The evaluation metrics are defined as follows:

$$Sensitivity = TP / (TP + FN) \quad (9)$$

$$Specificity = TN / (TN + FP) \quad (10)$$

$$DSC = 2TP / ((TP + FP) + (FN + TP)) \quad (11)$$

where the TP (true positive) is the region that is correctly identified as bone tissue, the FN (false negative) is the region that is incorrectly identified as non-bone tissue, the FP (false positive) is the region that is incorrectly identified as bone

tissue, and the TN (true negative) is the region which is correctly identified as non-bone tissue. The results were compared with the ground truth of the test data set. To perform model training and testing we have used NVIDIA GTX 1070 GPU of 8 GB RAM with 1920 cores as high computational power system.

A. Model Performance Results

The Mask R-CNN implementation was built in Python with libraries Keras and TensorFlow (Abadi *et al.,* 2016). The proposed algorithm is trained on 80 MR datasets with a total of 12,800 images. Then, the framework was tested on 10 datasets. The parameters such as momentum, learning rate, and epochs for Mask R-CNN are set up at 0.9, 0.0001, and 200, respectively. During training on the Mask R-CNN network, the learning rate is reduced by a factor of 10. The size of the fully connected layers in the classification graph is set as 1,024 for extracting knee bone class features. Our algorithm uses a bounding-box Non-max suppression threshold of 0.5 to filter RPN proposals. The RPN Anchor scales are set to (8, 16, 32, 64, 128) with an RPN anchor stride of one to detect knee bone class from input MR image. The decrease in the value of RPN Anchor scales leads to the detection of small bone class from MR images. However, too small RPN anchor scales miss out on larger knee bone instances. Table 1 shows the performance of the Mask R-CNN with Resnet-50 and Resnet-101 for sub chondral bone segmentation of femur, tibia and patella. The segmentation results obtained by using Mask R-CNN with Resnet-101 as backbone have better performance as compared to Resnet-50.

Table 1. Performance of Mask R-CNN with Resnet-50 and Resnet-101 for subchondral bone segmentation for ten datasets. Femur is denoted as F, tibia is denoted as T and patella is denoted as P.

	R-CNN with Resnet-50			**R-CNN with Resnet-101**		
	DSC	**Spec**	**Sens**	**DSC**	**Spec**	**Sens**
F	95.35	98.69	98.62	97.11	99.30	99.34
T	95.3	99.25	98.24	97.33	99.42	99.27
P	94.40	99.86	95.63	97.05	99.85	98.40

Table 2 shows the comparison of knee subchondral bone segmentation performance of baseline methods and Mask R-CNN algorithm on the OAI dataset. The Mask RCNN model with ResNet-50 back-bone achieved DSC of femur bone 95.35%, tibia bone 95.3%, and patella bone 94.40% on the validation dataset. Average DSC of femur bone 97.11%, tibia bone 97.33%, and patella bone 97.05% on the validation dataset by using Mask R-CNN with Resnet 101 as a backbone.

Table 2. The knee Bone Instance Segmentation results for the validation set

Method	**DSC SCORE**		
	F	**T**	**P**
(Zhou *et al.,* 2018)	97.00	96.20	89.80
(Liu *et al.,* 2018)	97.30	84.40	-
M-RCNN res-50	95.35	95.30	94.40
M-RCNN res-101	97.11	97.33	97.05

Figure 5 illustrates the effectiveness or robustness of the Mask RCNN framework for subchondral bone segmentation. In Mask R-CNN architecture is necessary to generate MR images and their respective ground truth labels into the MSCOCO style dataset for training and testing the proposed method. The Mask R-CNN architecture consists of backbone and head network used for feature extraction and instance segmentation, respectively. For the subchondral bone segmentation experiment, the proposed algorithm used Resnet-50 or Resnet-101 with FPN as a feature learning model referring to the backbone of Mask R-CNN. The total number of layers available in architecture is the key difference between Resnet-50 and Resnet-101 networks.

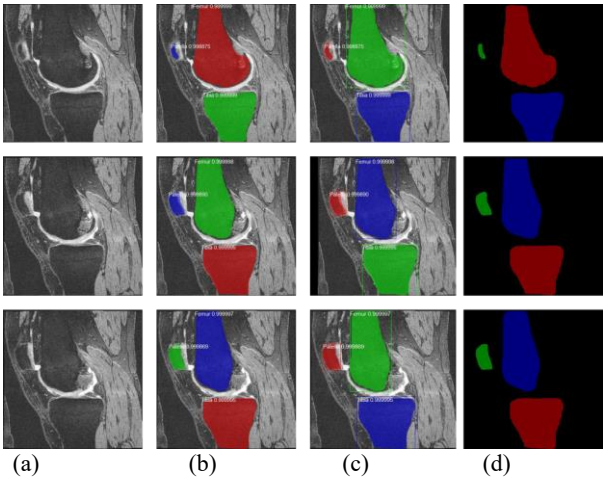

(a) (b) (c) (d)

Figure 5. Femur, patella, and tibia bones segmentation using the Mask RCNN. (a) MR-image sequence, (b) Bone mask with a class label for MR image, (c) Mask RCNN output for MR image, and (d) Bone mask with a background

From the experiment results, it was noticed that Resnet-50 with FPN has less computational load than ResNet-101 as a backbone in Mask RCNN. It was observed that the performance of ResNet-101-FPN has better accuracy and speed than the ResNet-50- FPN model as a backbone network. This performance improvement was obtained because ResNet-101-FPN has a better representation of the feature map than ResNet-50-FPN due to the extra number of deep convolutional layers.

The Top-down layers parameter is used to restore resolution with rich semantic information in bone instance segmentation. Therefore, the algorithm uses the size of the 256 top-down layers to create a features pyramid. The ROI Align layer was introduced in Mask R-CNN for improvement in pixel-level accuracy for instance segmentation. The mask prediction branch is a straightforward framework consisting of a fully convolutional layer with a soft mask of size 28x28 for fixed output. Then, the marching cube algorithm is introduced to 3D visualisation of knee subchondral bone. This algorithm helps to produce a triangle mesh by calculating iso-surfaces from discrete information. In the marching cube algorithm parameter like iso-value is set to 200 and the cube size value is the same as the number of pixels for the MR-Image slice.

IV. CONCLUSION

The problem of localisation, segmentation, and 3D visualisation of knee bone using MR-Images is tackled. The Mask R-CNN framework is selected to perform bone instance segmentation algorithms. Mask R-CNN can preserve spatial information due to its fully-connectivity between features learning approach and Mask Network for knee bone segmentation. The Mask R-CNN framework can obtain uniform knee subchondral bone detection and segmentation for each bone class due to the best suitable value of RPN Anchor scales. Top-down layer parameter and ROI align used to generate rich semantic information and improvement in pixel-level performance in knee subchondral bone instance segmentation. The segmented output from Mask R-CNN of 160 slices of MR images is a stack in parallel for the marching cube algorithm. The marching-cube algorithm is used for 3D knee subchondral bone visualisation by using MR images. The 3D knee subchondral bone is used for several applications such as knee replacement, monitor the risk stage for osteoarthritis, and determine treatment effects in trials of osteoarthritis.

V. ACKNOWLEDGEMENT

This research was financially supported by Fundamental Research Grant Scheme (FRGS) (Project title: Graph Transformed Deep 'Interactive' Learning Framework in Medical Image Segmentation, grant no: FRGS/1/2018/ICT02/UNIKL/02/4) provided by Ministry of Higher Education, Malaysia (MoHE), the Collaborative Research Grant Scheme (CRGS) provided by Centre of Research and Innovation (CoRI), Universiti Kuala Lumpur and Universiti Teknologi Malaysia, and Universiti Malaysia Kelantan Fundamental Grant (UMK Fund) (Project title: Attention-Based Generative Adversarial network for Realistic Knee Image Synthesis), grant no: R/FUND/A1500/01934A/2022/01043.

VI. REFERENCES

Abadi, M, Barham, P, Chen, J, Chen, Z, Davis, A, Dean, J, Devin, M, Ghemawat, S, Irving, G, Isard, M & Kudlur, M 2016, 'Tensorflow: A system for large-scale machine learning. In 12th {USENIX} symposium on operating systems design and implementation ({OSDI} 16)', pp. 265-283.

Abdulla, W 2017, Mask r-cnn for object detection and instance segmentation on keras and tensorflow.

Ambellan, F', Tack, A, Ehlke, M & Zachow, S 2019, 'Automated segmentation of knee bone and cartilage combining statistical shape knowledge and convolutional neural networks: Data from the Osteoarthritis Initiative', Medical Image Analysis, vol. 52, pp. 109-118.

Barr, AJ, Dube, B, Hensor, EM, Kingsbury, SR, Peat, G, Bowes, MA, Sharples, LD & Conaghan, PG 2016, 'The relationship between three-dimensional knee MRI bone

shape and total knee replacement—a case control study: data from the Osteoarthritis Initiative', Rheumatology, vol. 55, no. 9, pp. 1585-1593.

Bowes, MA, Vincent, GR, Wolstenholme, CB & Conaghan, PG 2015, 'A novel method for bone area measurement provides new insights into osteoarthritis and its progression', Annals of the Rheumatic Diseases, vol. 74, no. 3, pp. 519-525.

Deniz, CM, Xiang, S, Hallyburton, RS, Welbeck, A, Babb, JS, Honig, S, Cho, K & Chang, G 2018, 'Segmentation of the proximal femur from MR images using deep convolutional neural networks', Scientific Reports, vol. 8, no. 1, pp. 1-14.

Gait, AD, Hodgson, R, Parkes, MJ, Hutchinson, CE, O'Neill, TW, Maricar, N, Marjanovic, EJ, Cootes, TF & Felson, DT 2016, 'Synovial volume vs synovial measurements from dynamic contrast enhanced MRI as measures of response in osteoarthritis', Osteoarthritis and Cartilage, vol. 24, no. 8, pp. 1392-1398.

Girshick, R 2015, 'Fast R-CNN', in Proceedings of the IEEE International Conference on Computer Vision, pp. 1440-1448.

Girshick, R, Donahue, J, Darrell, T & Malik, J 2014, 'Rich feature hierarchies for accurate object detection and semantic segmentation', in Proceedings of the IEEE Conference on Computer Vision and Pattern Recognition, pp. 580-587.

He, K, Gkioxari, G, Dollár, P & Girshick, R 2017, 'Mask R-CNN', in Proceedings of the IEEE International Conference on Computer Vision.

Hong-Seng, G, Khairil Amir, S & Abdul Helmy, AK 2017, 'Investigation of random walks knee cartilage segmentation model using inter-observer reproducibility: Data from the Osteoarthritis Initiative', Bio-Medical Materials and Engineering, vol. 28, no. 2, pp. 75-85

Hong-Seng, G, Khairil Amir, S, Muhammad Hanif, R, Yeng-Seng, Lee, Wan Mahani, WM & Abdul Helmy, AK 2019, 'Unifying the seeds auto-generation (SAGE) with knee cartilage segmentation framework: Data from the Osteoarthritis Initiative', Bio-Medical Materials and Engineering, vol. 28, no. 2, pp. 75-85

Hong-Seng, G, Muhammad Hanif, R, Asnida Wahad, W, Yeng-Seng, Lee & Akinobu, S 2020, 'From Classical to deep learning: review on cartilage and bone segmentation techniques in knee osteoarthritis research', Artificial Intelligence Review, vol. 54, pp. 2445-2494.

Hong-Seng, G, Tian-Swee, T, Khairil Amir, S, Abdul Helmy, AK & Mohammed Rafiq, AK 2014, 'Multilabel graph based approach for knee cartilage segmentation: Data from the Osteoarthritis Initiative', in IEEE Conference on Biomedical Engineering and Sciences, pp. 201-213.

Lee, H, Hong, H & Kim, J 2018, April, 'BCD-NET: A novel method for cartilage segmentation of knee MRI via deep segmentation networks with bone-cartilage-complex modeling', in 2018 IEEE 15th International Symposium on Biomedical Imaging (ISBI 2018), IEEE, pp. 1538-1541.

Lin, G, Milan, A, Shen, C & Reid, I 2017, 'Refinenet: Multi-path refinement networks for high-resolution semantic segmentation', in Proceedings of the IEEE Conference on Computer Vision and Pattern Recognition, pp. 1925-1934.

Lin, TY, Maire, M, Belongie, S, Hays, J, Perona, P, Ramanan, D, Dollár, P & Zitnick, CL 2014, September, 'Microsoft coco: Common objects in context', in European Conference on Computer Vision, Springer, Cham, pp. 740-755.

Liu, F, Zhou, Z, Jang, H, Samsonov, A, Zhao, G & Kijowski, R 2018, 'Deep convolutional neural network and 3D deformable approach for tissue segmentation in musculoskeletal magnetic resonance imaging', Magnetic Resonance in Medicine, vol. 79, no. 4, pp. 2379-2391.

Lorensen, WE & Cline, HE 1987, 'Marching cubes: A high resolution 3D surface construction algorithm', ACM Siggraph Computer Graphics, vol. 21, no. 4, pp. 163-169.

MacKay, JW, Murray, PJ, Kasmai, B, Johnson, G, Donell, ST & Toms, AP 2017, 'Subchondral bone in osteoarthritis: association between MRI texture analysis and histomorphometry', Osteoarthritis and Cartilage, vol. 25, no. 5, pp. 700-707.

Neogi, T & Felson, DT 2016, 'Bone as an imaging biomarker and treatment target in OA', Nature Reviews Rheumatology, vol. 12, no. 9, pp. 503-504.

Peterfy, CG, Schneider, E & Nevitt, M 2008, 'The osteoarthritis initiative: report on the design rationale for the magnetic resonance imaging protocol for the knee', Osteoarthritis and Cartilage, vol. 16, no. 12, pp. 1433-1441

Ren, S, He, K, Girshick, R & Sun, J 2015, 'Faster R-CNN: Towards real-time object detection with region proposal networks', arXiv preprint arXiv:1506.01497.

Zhou, Z, Zhao, G, Kijowski, R & Liu, F 2018, 'Deep convolutional neural network for segmentation of knee joint anatomy', Magnetic Resonance in Medicine, vol. 80, no. 6, pp. 2759-2770.